AGU100 ADVANCING EARTH AND SPACE SCIENCE

Water Resources Research

RESEARCH ARTICLE
10.1002/2017WR021682

Key Points:
- In wet, energy-limited regions, evapotranspiration uncertainty is high regarding both representation of annual cycles and anomalies
- Dry, water-limited regions show maximum uncertainty of annual mean evapotranspiration, but products agree better on anomaly occurrence
- Land surface models detect all agricultural droughts reported in literature while the remote sensing products do not always detect them

Correspondence to:
A. A. Sörensson,
sorensson@cima.fcen.uba.ar

Citation:
Sörensson, A. A., & Ruscica, R. C. (2018). Intercomparison and uncertainty assessment of nine evapotranspiration estimates over South America. *Water Resources Research*, *54*, 2891–2908. https://doi.org/10.1002/2017WR021682

Received 9 AUG 2017
Accepted 19 MAR 2018
Accepted article online 24 MAR 2018
Published online 16 APR 2018

Intercomparison and Uncertainty Assessment of Nine Evapotranspiration Estimates Over South America

Anna A. Sörensson[1] and Romina C. Ruscica[1]

[1]Centro de Investigaciones del Mar y la Atmósfera, CONICET/UBA, UMI IFAECI/CNRS, Buenos Aires, Argentina

Abstract This study examines the uncertainties and the representations of anomalies of a set of evapotranspiration products over climatologically distinct regions of South America. The products, coming from land surface models, reanalysis, and remote sensing, are chosen from sources that are readily available to the community of users. The results show that the spatial patterns of maximum uncertainty differ among metrics, with dry regions showing maximum relative uncertainties of annual mean evapotranspiration, while energy-limited regions present maximum uncertainties in the representation of the annual cycle and monsoon regions in the representation of anomalous conditions. Furthermore, it is found that land surface models driven by observed atmospheric fields detect meteorological and agricultural droughts in dry regions unequivocally. The remote sensing products employed do not distinguish all agricultural droughts and this could be attributed to the forcing net radiation. The study also highlights important characteristics of individual data sets and recommends users to include assessments of sensitivity to evapotranspiration data sets in their studies, depending on region and nature of study to be conducted.

1. Introduction

Terrestrial evapotranspiration (ET) is a key variable of the climate system that interconnects the water, energy, and carbon budgets of the land surface (e.g., Jung et al., 2010; Wang & Dickinson, 2012). Improved estimates of evapotranspiration are crucial both for a large variety of practical applications and for a better theoretical understanding of current and future water/energy/carbon budgets and their interaction with the climate on a wide range of temporal and spatial scales. Because of its central role, ET is crucial for the validation and development of climatic, hydrologic, and vegetation models.

ET can be estimated through various methods, spanning from point scale observations with very fine temporal resolution, to remote sensing products and process modeling with global coverage but coarser spatiotemporal resolution (Wang & Dickinson, 2012). The FLUXNET network (Baldocchi et al., 2001) recollects and provides flux measurements around the world, which are frequently used for calibrating and validating coarser-scale global data sources. However, some regions, like South America, are still very poorly covered with flux towers. ET products derived from remote sensing data (RS) are based on different approaches, including the combination of RS data with simple atmosphere-land exchange models (e.g., Mecikalski et al., 1999), empirical and statistical methods based on RS surface temperature data (e.g., Kalma et al., 2008), and vegetation index methods (e.g., Glenn et al., 2010). ET can also be estimated using land surface models (LSMs), which are based on fundamental biophysical and, depending on the complexity of the model, biogeochemical processes (e.g., Pitman, 2003). LSMs can be used to obtain estimates of ET of past and present climate when forced by observed atmospheric data or be coupled to climate models to estimate ET under future climate change scenarios (Getirana et al., 2014; Ruscica et al., 2016).

Improved knowledge of the performance of existing tools for monitoring and forecasting ET in South America are important for diverse hydrological and agricultural applications such as water consumption for irrigation and livestock, electricity production and human use (Barros et al., 2003). ET is a main driver of drought in some climates (e.g., Teuling et al., 2013) and regions such as northeastern Brazil and the eastern hillside of the central and southern Andes suffer water scarcity due to large precipitation interannual and interdecadal variability, high potential evapotranspiration, and glacier and snow pack melting that could be aggravated in future climate (Marengo & Bernasconi, 2015; Masiokas et al., 2006, 2009; Rivera et al., 2013). ET is also highly relevant for temperature variability and hot extremes (e.g., Mueller & Seneviratne, 2012; Hirschi

et al., 2011; Seneviratne et al., 2006; Yin et al., 2014). Large areas of South America are suffering rapid land use transformations with consequences for the water budget through changes in infiltration, runoff, and transpiration regimes, contributing to flooding and droughts (Germer et al., 2009; Lima et al., 2014; Nosetto et al., 2015; Silveira & Alonso, 2009).

Evapotranspiration also plays an important role for large-scale climatic features over the continent. The increment of latent heat flux at the end of the dry season over the Amazon region contributes to the triggering of the South American Monsoon System onset (Li & Fu, 2004). This increase in ET has been linked to leaf development and demography, suggesting intrinsic interactions between rainforest phenology and climate (Wu et al., 2016). The evapotranspiration from Amazonia is important not only locally; studies have estimated that moisture with origin in Amazonia contributes to 25–70% of precipitation in southeastern South America (Dirmeyer et al., 2009; Martinez & Dominguez, 2014; van der Ent et al., 2010).

A better knowledge of ET is crucial for limiting the uncertainties of future climate projections. Boé and Terray (2008) showed that the responses of ET to climate change differ among climate models due to their different parameterizations that connect soil moisture and surface radiation to ET. This results in uncertainties in the magnitude of temperature changes through the different partitioning of energy at the surface. In particular, regions of strong interaction between soil moisture and atmosphere in future climate such as southeastern South America and Cerrado in Brazil (Ruscica et al., 2016) could be affected by such feedbacks.

ET from different sources has been compared on a global scale (e.g., Jiménez et al. 2011; Michel et al., 2016; Miralles et al., 2016; Mueller et al., 2013; Vinukollu et al., 2011) and over the Amazon Basin (e.g., Fisher et al., 2009; Getirana et al., 2014). However, there is a lack of detailed knowledge on the regional scale which is fundamental, e.g., impact studies and continental scale phenomena such as the transport of humidity from the Amazon to the southeastern South America. The aim of this paper is to assess the behavior and uncertainty of ET over South America from some of the most common available gridded products, taking into account the wide variety of climatic regimes of the continent. We have chosen products from the following three categories: LSMs, reanalysis, and RS. The following questions are addressed: (1) How well do the products agree on mean climate and anomaly representation? (2) Do the products detect hydrological extremes such as droughts? (3) How do different products respond to anomalies of precipitation and net surface radiation? Answering these questions reveal strengths and weaknesses of the ET products over the different climatic regions of the continent, knowledge that can be useful for different scientific and practical purposes.

The paper is organized as following: in section 2, the division in climatic regions and the products are presented. In section 3, the results are displayed: section 3.1 treats multiannual mean behavior and uncertainty, section 3.2 the representation and uncertainty of anomalies, section 3.3 the detection of droughts, and section 3.4 the response of the different ET products to precipitation and net surface radiation anomalies. Summary and conclusions are given in section 4.

2. Materials and Methods

2.1. Selection of Climatic Regions

The water and energy budget equations can be written:

$$ET = P - R - dw/dt, \tag{1}$$

$$\lambda ET = Rn - H - G, \tag{2}$$

where P is precipitation, R runoff, dw/dt change of soil water storage, λ latent heat of vaporization, λET latent heat flux, Rn net radiation at the surface, H sensible heat flux, and G is the ground heat flux. ET is composed of evaporation from surfaces (e.g., soil, water bodies, and vegetation) and plant transpiration, the latter being the connection to the carbon budget due to its coupling to photosynthesis.

From a climatic viewpoint we will use the concepts of *water-limited* versus *energy-limited* ET regimes (e.g., Seneviratne et al., 2010). Water-limited regions are arid to semiarid where ET is limited by available soil moisture which is driven principally by precipitation. Energy-limited regions have abundant precipitation and soil humidity, and the main limiting factor of ET is atmospheric moisture demand. The two regimes are not necessarily static over time but can have an annual cycle or change irregularly due to interannual

variability of the water cycle, in particular over transition zones between dry and wet climates such as southeastern South America (Ruscica et al., 2015). Furthermore, ET products do not necessarily represent the two regimes well. In LSMs, this can be due to insufficient water storage or rooting depth that limits transpiration during dry periods (e.g., in southern Amazonia during the dry season JJA; Christoffersen et al., 2014; Yang et al., 2016), erroneous vegetation cover (interannual variability of vegetation properties and seasonal cycle of crops are often not included; Müller et al., 2014), and lack of representation of wetlands (e.g., Pantanal; Hamilton, 2002) or irrigation (southern Brazil; Barros et al., 2003), among others. Reanalysis products share these sources of errors and furthermore they suffer large precipitation biases over many regions. RS products based on vegetation indices have the advantage of capturing variability of vegetation properties, crops, irrigations, and flooding but have a tendency to underestimate the water limitation on ET since ET is not restricted by the water balance equation like in LSMs (e.g., Long et al., 2014).

Equations (1) and (2) reveal precipitation (P) and net surface radiation (Rn) as main drivers of ET. To find regions with similar spatial and temporal characteristics of ET we defined regions based on the annual cycles of these two drivers applying a K-means clustering analysis to the annual cycles of P and Rn for 1984–2007.

Figure 1 shows the regions together with their mean annual cycles of P and Rn (from GPCP and SRB, see section 2.2). The Northern South America (NSA, Figure 1a), Equator (EQ, Figure 1b), and southern Amazon (SAmz, Figure 1c) regions show weak annual cycles of radiation which are clearly influenced by the cloudiness related to high precipitation (see the relative Rn minimum/P maximum of AMJJ in NSA, Rn maximum/P minimum of ASO in EQ and the relative Rn minimum/P maximum of ND in SAmz). NSA and EQ have large intergrid point spreads of precipitation, however, the shapes of the annual cycle of precipitation of all grid points are similar within each region (not shown). The annual cycle of radiation of the other six regions follows the solar cycle with large differences in amplitude since annual minimum Rn varies between 105 W/m^2 in northeastern Brazil (NeB, Figure 1d) and 5 W/m^2 in Patagonia (PAT, Figure 1i). SAmz as well as the South American Monsoon System region (SAMS, Figure 1e) and Andes (Figure 1g) regions have clear monsoon regimes while Central Argentina (CArg, Figure 1h) has a less pronounced dry season. Southeastern South America (SESA, Figure 1f) has precipitation all year and PAT is characterized by arid conditions with winter maximum.

2.2. Precipitation and Net Surface Radiation Products

To account for observational uncertainty of P and Rn we used four products for P: GPCP, CRU, UDEL, and CPC for P and two for Rn: SRB and CLARA. See details and references for each product in Table 1. Since annual cycles of both variables were similar among these products (not shown) the clustering was realized with GPCP and SRB. For our purpose we found that the precipitation products were similar also with respect to sign of seasonal anomalies with some differences in magnitude. Therefore, to construct seasonal P anomaly time series, the time series of the seasonal means of the four products were averaged and the anomaly was calculated from the resulting series (P_{Ens}). On the contrary, SRB and CLARA show very different temporal evolution of anomalies, frequently differing in sign (for differences between SRB and CLARA see also Loew et al., 2016). Therefore, we calculate and analyze the Rn anomalies separately for each product.

2.3. Evapotranspiration Products

The nine ET products used in this study are detailed with references in Table 1. The three LandFlux products "LSM," "Reanalysis," and "Diagnostic" (Mueller et al., 2013, hereafter LF) limit the period of this study to 17 years (1989–2005). The LF-Diagnostic product (hereafter LF-RS) consists of data from RS, in situ measurements and a water balance diagnostic estimate; however, here it is considered as a RS product since the in situ data for South America is practically nonexistent (few stations, each with only a few months available, Jung et al., 2009) and the water balance estimate does not include South America (Mueller et al., 2011).

All products were interpolated to the grid of GPCP which is the product with the coarsest grid in this study (2.5° × 2.5°).

2.4. The Similarity Index

To quantify how well the ET products coincide on the representation of the temporal evolution of ET, the "similarity index" Ω is employed (Yamada et al., 2007). Ω quantifies how similar the members of an ensemble of time series are with respect to their phase, mean value and amplitude.

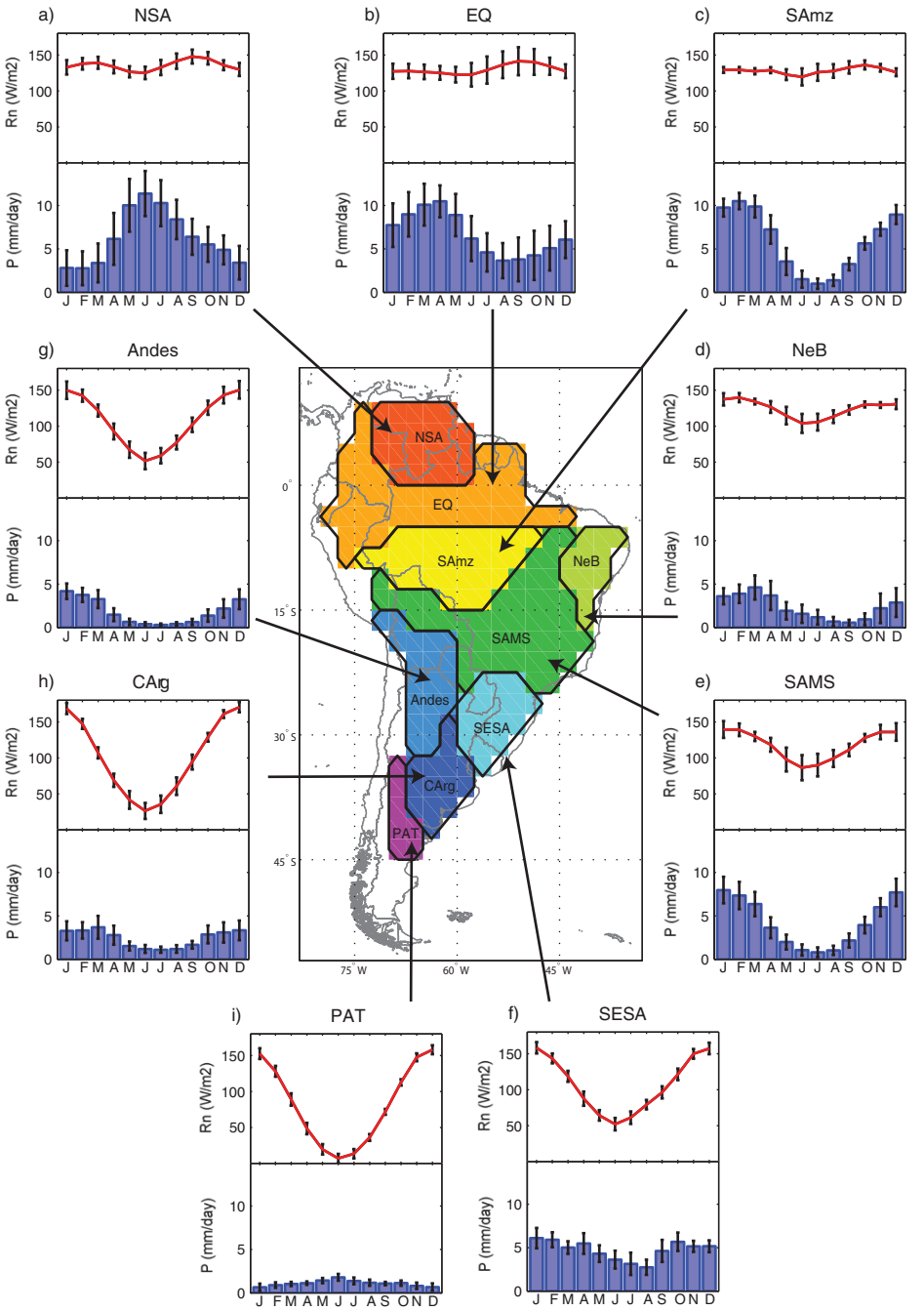

Figure 1. (middle) Regions of study based on the areal mean annual cycles of (a–i) (top) net surface radiation (units: W/m^2) and (a–i) (bottom) precipitation (units: mm/d). Error bars reflect intergrid point standard deviation of each region.

$$\Omega = \frac{m\sigma_b^2 - \sigma^2}{(m-1)\sigma^2}, \tag{3}$$

where m is the number of ensemble members, σ_b^2 is the variance of the time series that results from calculating the ensemble mean of each time step, and σ^2 is the total variance of all members concatenated. Ω has values between 0 (no similarity among the series at all) and 1 (for identical series).

Water Resources Research

10.1002/2017WR021682

Table 1
ET, P, and Rn Products Used for This Study

Variable/type of product	Name (abbreviation)	Product characteristics	Resolution (°, temporal)	References
Evapotranspiration (ET)/ off-line land surface models (LSMs)	Era-Interim-Land (ERAI-L)	HTESSEL LSM (Hydrology-Tiled ECMWF Scheme for Surface Exchanges over Land) forced by ERA-Interim atmospheric forcing, GPCP based correction of monthly precipitation. Soil depth 2.89 m, four soil layers, vegetation data from ECOCLIMAP.	0.75 × 0.75 daily	Balsamo et al. (2015). For HTESSEL, see Balsamo et al. (2009), for ECOCLIMAP, see Masson et al. (2003).
	Global Land Data Assimilation System version 2 (GLDAS2)	Noah LSM forced by Goddard Earth Observing System (GEOS) Data Assimilation System with corrected precipitation and radiation. Soil depth 2 m, four soil layers, vegetation data from University of Maryland (http://glcf.umd.edu/data/landcover/).	0.25 × 0.25 monthly	Rodell et al. (2004). For Noah, see Ek et al. (2003), for forcing data, see Sheffield et al. (2006).
	Modern-Era Retrospective Analysis for Research and Applications-Land (MERRA-L)	GEOS-5 Catchment LSM forced by MERRA with corrected precipitation. Base unit of LSM is watershed (as differing from the common grid point approach). Soil depth 0.75–1 m, two soil layers, vegetation data from GEOS-5.	0.67 (lon) × 0.5 monthly	Reichle et al. (2011). For Catchment LSM, see Koster et al. (2000), for GEOS-5, see Rienecker et al. (2011).
	LandFLux-LSM (LF-LSM)	Ensemble of five realizations of four off-line LSMs forced by reanalysis corrected by observational data. The ensemble includes MERRA-L, used in this study.	1 × 1 monthly	Mueller et al. (2013).
Evapotranspiration (ET)/ reanalysis (REA)	ECMWF Reanalysis-Interim (ERAI)	TESSEL LSM (Tiled ECMWF Scheme for Surface Exchanges over Land). Soil depth 2.89 m, four soil layers, high and low vegetation from the Global Land Cover Characteristics (GLCC).	0.75 × 0.75 monthly	Dee et al. (2011). For TESSEL, see Viterbo and Beljaars (1995), for GLCC, see Loveland et al. (2000).
	LandFlux-Reanalysis (LF-REA)	Ensemble of four reanalysis, including ERAI, used in this study.	1 × 1 monthly	Mueller et al. (2013)
Evapotranspiration (ET)/ remote sensing product (RS)	Process-based Land Surface Evapotranspiration/ heat fluxes algorithm (P-LSH)	Normalized Difference Vegetation Index (NDVI)-based Penman-Monteith model. Canopy evapotranspiration, soil evaporation, and evaporation from open water bodies are computed separately. Surface meteorological information from NCEP/NCAR reanalysis, SRB surface solar radiation and NDVI from NOAA-AVHRR Global Inventory Modeling and Mapping Studies.	1 × 1 monthly	Zhang et al. (2010). For NCEP/NCAR, see Kalnay et al. (1996), for SRB, see Stackhouse et al. (2013) and Zhang et al. (2013), for NOAA-AVHRR, see Pinzon et al. (2005).
	Priestley-Taylor Jet Propulsion Laboratory model (PT-JPL)	Priestly-Taylor model where plant temperature and moisture constraint factors have been introduced. PT-JPL uses Rn, NDVI, maximum air temperature, and water vapor pressure from ISLSCP-II and a soil adjusted vegetation index from AVHRR.	1 × 1 monthly	Fisher et al. (2008). For ISLSCP-II, see Los et al. (2000), for NOAA-AVHRR, see Pinzon et al.(2005).
	LandFlux-diagnostic (LF-RS)	Ensemble of seven diagnostic products.	1 × 1 monthly	Mueller et al. (2013).
Precipitation (P)	Global Precipitation Climatology Project (GPCP)	Gauge combined with satellite.	2.5 × 2.5 monthly	Adler et al. (2003).
	Global Unified Gauge-Based Analysis of Daily Precipitation (CPC-UNI)	Gauge(land)-Based Analysis.	0.5 × 0.5 monthly	Chen et al. (2008).
	University of Delaware (UDEL)	Gauge (land) data.	0.5 × 0.5 daily	Willmott and Matsuura (2001).
	University of East Anglia Climatic Research Unit (CRU)	Gauge (land) data.	0.5 × 0.5 monthly	Harris and Jones (2015).
Net surface radiation (Rn)	CM SAF CLARA-A1 (CLARA)	Satellite based.	0.25 × 0.25 monthly	Karlsson et al. (2013).
	NASA/GEWEX Surface Radiation Budget Release-3.0 (SRB)	Satellite based.	1 × 1 monthly	Stackhouse et al. (2011) and Zhang et al. (2013).

3. Results and Discussion

3.1. Annual Means and Seasonal Cycle

Figure 2 shows the annual ensemble mean (a), spread (b), spread excluding MERRA-L (c), and the annual mean ET for each individual product (d–l). The spread is defined as the range between the maximum and minimum of the ensemble and can be interpreted as the maximum uncertainty that choosing a random product to represent annual mean ET would introduce in a study. While the products share large-scale spatial patterns such as maximum in Amazonia and local minima in NeB, PAT, and Andes, the uncertainties are, as seen in Figure 2b, as large as 1.5–2 mm/d in regions with ensemble mean values of 2.5–4 mm/d (Figure 2a). Maximum uncertainty in Figure 2b does not coincide with the maximum ET values over Amazonia but shows two maxima, one over the very southwestern Amazonia and the other over central Brazil. Noting that MERRA-L has very large ET values over these regions (Figure 2i) the spread was re computed excluding this product (Figure 2c), obtaining maximum uncertainty centered on the border between Bolivia, Brazil, and Paraguay. This region has a strong monsoon regime and sharp spatial gradient of precipitation (Ruscica et al., 2016, their Figure 1) and some of the discrepancy among the products could therefore come from different simulated precipitation in the reanalysis products (Figures 2e and 2j). Northern NSA also stands out as a region with large uncertainty, due to low ET of LF-LSM and P-LSH. LF-LSM shows a local minimum in central Amazonia that is not shared by any other product. The pattern in Figure 2c seems to be

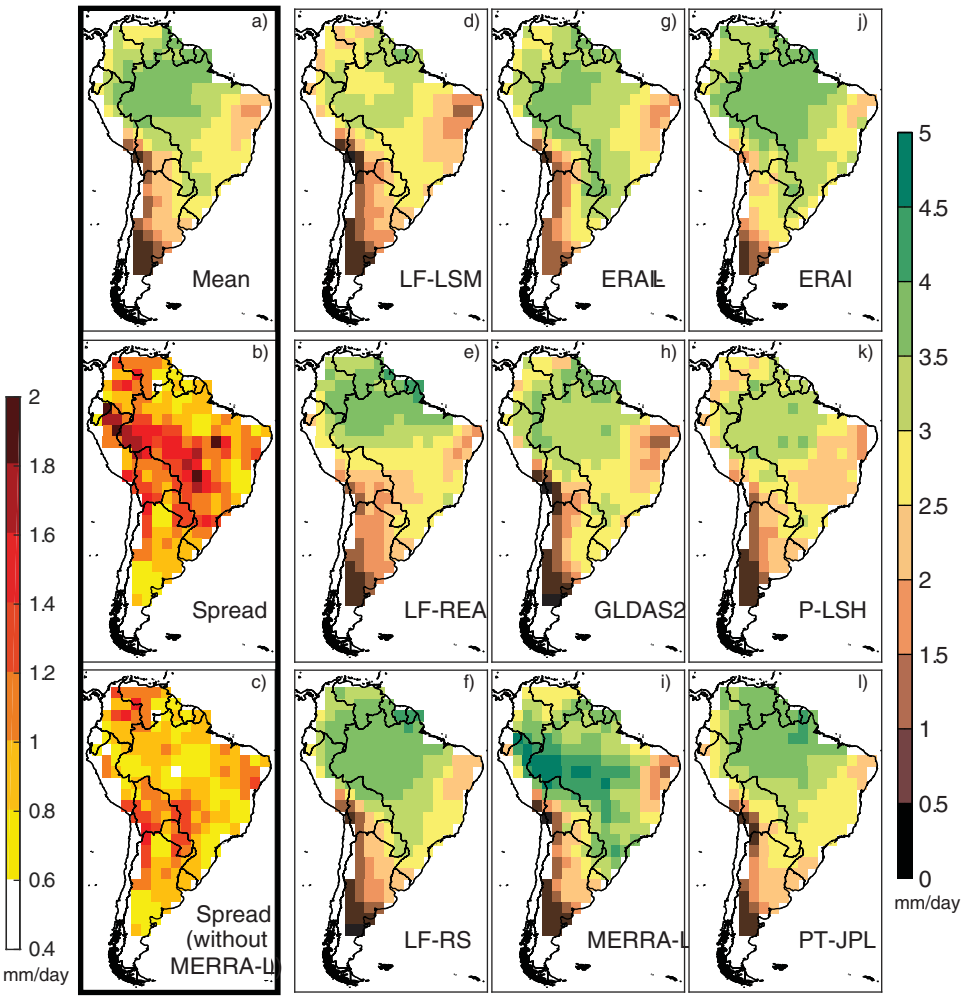

Figure 2. ET annual fields. (a) Ensemble mean, (b) ensemble spread—defined as the difference between ensemble maximum and minimum, (c) ensemble spread excluding the product MERRA-L, and (d–l) mean of each ensemble member, units: mm/d.

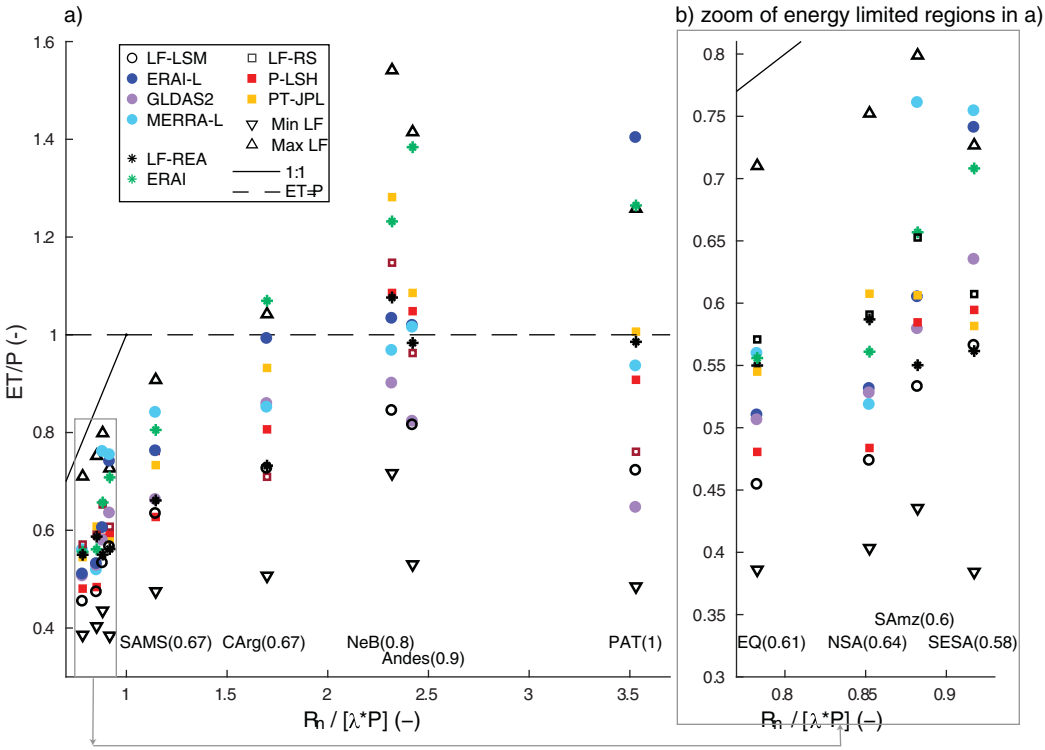

Figure 3. (a) Scatterplots of annual means of ET/P and Rn/λP of each region and ET data set. (b) The zoom of the four most humid regions in Figure 3a. Numbers in parentheses after the name of each region indicate the ET ensemble spread relative to the ensemble mean as a measure of uncertainty.

robust since it is similar to Jiménez et al. (2011, their Figure 3) who compared global latent heat flux from 12 products of which only ERA-Interim participates in our study. The uncertainty estimate of global ET of Vinukollu et al. (2011, their Figure 8) also shares main characteristics with our results.

Figure 3 links the uncertainty of annual mean ET to the location of each region and product in the Budyko space (Budyko, 1982). The Budyko space relates the annual ratio ET/P to the aridity index Ep/P, where Ep is defined as Ep = Rn/λ and P and Rn are computed as the mean of the observational P and Rn in Table 1. The circles, stars, and squares correspond to the individual products' means and the triangles correspond to the minimum and maximum values of the full LandFlux-EVAL ensemble. ET is restricted to the space below both the dashed line that represents the ET = P and the full line that represents ET = Ep. The number in parenthesis after the name of each region is a measure of the relative uncertainty of ET, defined as the total spread among the products divided by the mean ET. The highest relative uncertainty occurs in PAT (1.0), and the lowest in SESA (0.58).

For the four water-limited regions several products show annual ET equal to or even considerably higher than precipitation. For ERAI, this is because of its overestimation of rainfall in the Andes and CArg regions (Dee et al., 2011). The monthly GPCP based correction of ERAI precipitation used to force ERAI-L (Balsamo et al., 2015) is probably one of the reasons for a lower ET in ERAI-L than in ERAI in these regions. However, ERAI-L overestimates ET in PAT probably because GPCP overestimates P with respect to the other databases in this region (not shown). In the case of RS products, both P-LSH and PT-JPL overestimate ET in Andes and NeB (PT-JPL also overestimates ET slightly in PAT). For P-LSH, this is consistent with the global evaluation of this product based on water balance (Zhang et al., 2010) that showed a tendency to overestimate ET in arid environments and underestimate in wet environments. The PT-JPL model was evaluated against flux tower data globally by Zhang et al. (2017) who found that the model systematically overestimates ET in arid regions. LF-RS is high in NeB and is responsible for the maximum of LF-products in Andes and NeB (not shown). A possible explanation for this could be that some RS products in the LF-ensemble do not include explicit water limiting restriction (Long et al., 2014; Yang et al., 2015).

ERAI is on the higher end of ET estimations also in energy-limited regions. Miralles et al. (2016) confirms this on a global scale; among 11 different products and methods ERAI has the highest global mean. ERAI-L lowers the ERAI estimate also in energy-limited regions, where the change to the hydrology in ERAI-L that increases surface runoff (Balsamo et al., 2015) could contribute. MERRA-L shows very high ET values over energy-limited regions. In the global study of Jiménez et al. (2011), it was found that MERRA estimates large Rn and λET values over wet regions as compared to RS, reanalysis and LSM products. The fact that radiation from MERRA used to force MERRA-L is not corrected (Reichle et al., 2011) can contribute to the high values obtained here. Consistently with Zhang et al. (2010), the P-LSH product is on the low end of the ET estimates in energy-limited regions. The mean of LF-LSM is on the very low end of ET estimates for all regions, which has also been confirmed on a global scale by Mueller et al. (2013).

The annual cycles of the areal mean ET of each product and region are shown in Figure 4. In NSA, the RS products show a large spread (Figure 4-3). All products agree however in that the peak of ET occurs after the wet season, during the second maximum of radiation (September–October, Figure 1a). The first maximum of radiation (February–March, Figure 1a) occurs after and during the annual precipitation minimum and since all products show less evapotranspiration than during the second maximum this indicates that ET could be water-limited during these months. In EQ, the radiation maximum occurs in September–October and the precipitation maximum in March–April (Figure 1b). The ET products show two types of annual cycles. ERAI-L, LF-REA, PT-JPL, and LF-RS show a flat curve with a slight maxima during the rainy March–April (Figures 4-4–4–6), suggesting water limitation which could be the case for southern EQ which is dry during this period (not shown). On the other hand, MERRA-L, GLDAS2, LF-LSM, ERAI, and P-LSH follow the annual cycle of radiation, a behavior that coincides more with flux tower observations in the equatorial forest in eastern Amazonia (Christoffersen et al., 2014).

SAmz is the region where ET estimations generally show the highest discrepancy (Figures 4–7–4–9). The high annual values of MERRA-L seen in Figures 2 and 3 are caused by very large monthly ET except during the dry months of July–September. This is probably caused by interactions between the assimilated observations and cloud/radiation in the forcing data sets (Bosilovich, personal communication, 2015). GLDAS2 has much smaller amplitude but shows the same sharp drop of ET in July–September. LF-REA (Figure 4–8) and PT-JPL (Figure 4–9) coincide on minimum during July–September but have a smoother cycle. LF-REA shows a very low minimum ensemble value of (1 mm/d). ERAI-L and LF-RS (Figure 4–9) agree on earlier ocurrence of the minimum. These six products (MERRA-L, GLDAS2, LF-REA, PT-JPL, ERAI-L, and LF-RS) suggest that SAmz has water-limited behavior during the dry months, while on the contrary one product from each category: LF-LSM, ERAI, and P-LSH show maximum during or after the precipitation minimum, suggesting an energy-limited behavior the whole year which is more consistent with flux tower observations (Christoffersen et al., 2014). Mechanisms that regulate water supply and demand in this region during the dry season are still poorly understood (Christoffersen et al., 2014) and ET estimates of LSM studies diverge due to different formulations of physical processes (Getirana et al., 2014). The LSM products here do not include important processes on the water supply side such as groundwater (Miguez-Macho & Fan, 2012) and deep roots (Yang et al., 2016) and this is probably the reason why four out of six LSM-based products in this study show a water-limited behavior in the dry season. Christoffersen et al. (2014) showed that various LSMs eliminate the dry season bias by including either of these two processes. There is also a discussion on whether climate or vegetation phenology governs the demand side. Using flux tower measurements, Fisher et al. (2009) showed that radiation was the outstanding strongest determinant of ET regardless of season while Costa et al. (2010) and Wu et al. (2016) argue that seasonally varying demand of vegetation could play an important role, especially during the dry season. Phenology however is poorly represented in most models (e.g., Christoffersen et al., 2014), including those of this study.

In water-limited NeB, radiation is abundant all-year-round and all products agree on that ET follows the precipitation annual cycle (Figures 4–10–4–12). In the monsoon dominated regions SAMS (Figures 4–13–4–15) and Andes (Figures 4–19–4–21), precipitation, radiation, and ET follow the same annual behavior. In SESA (Figures 4–16–4–18) and CArg (Figures 4–22–4–24), ET follows the solar cycle. In PAT (Figures 4–25–4–27), rainfall peaks in winter, but due to very limited energy input during winter, ET peaks in spring and summer.

In summary, although the products show very large differences in mean annual ET, products agree well on simulating the amplitude and timing of the annual cycle both in the southern regions that have well defined annual cycles of radiation, and in NeB that is not limited by radiation but by precipitation

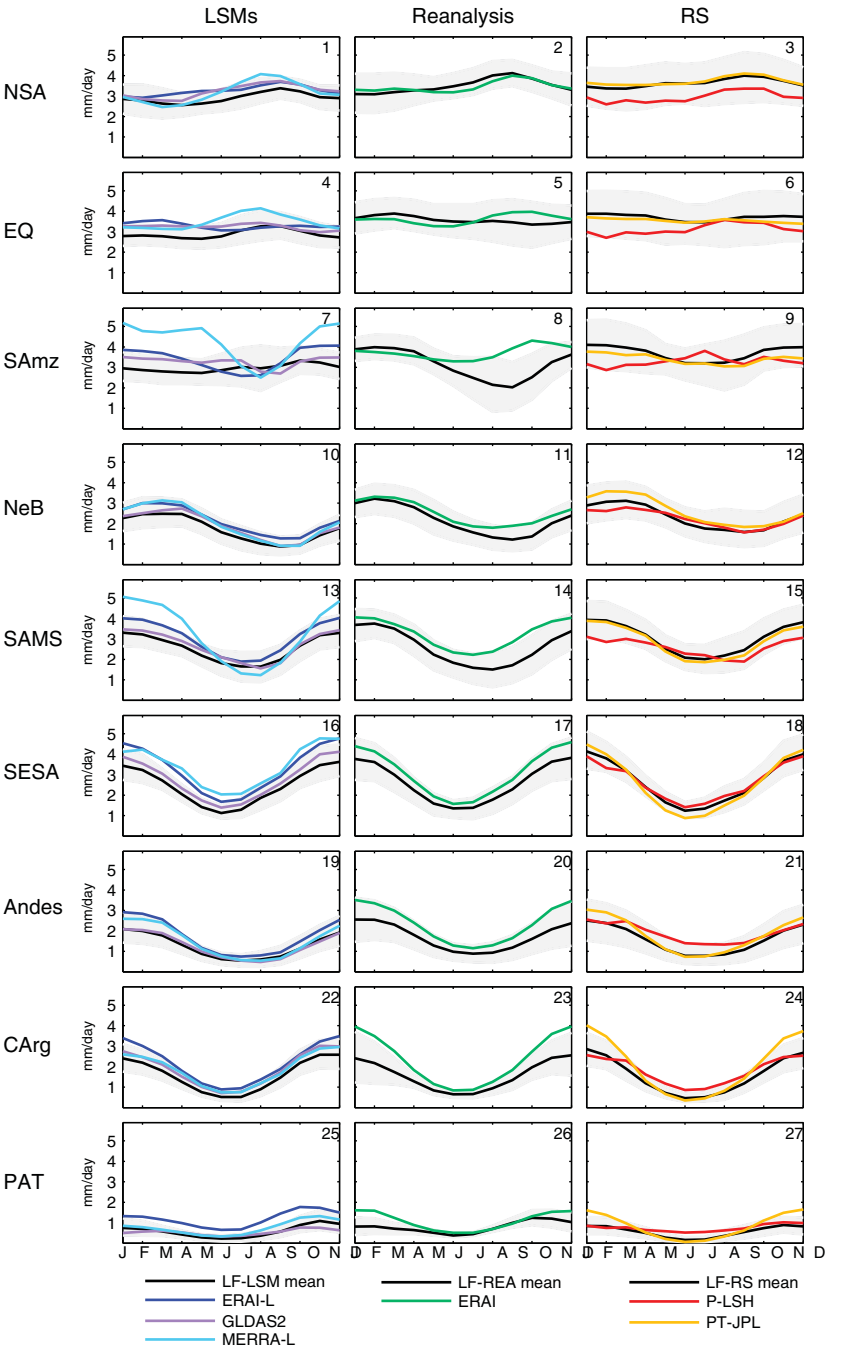

Figure 4. (rows) ET annual cycles for each region and category of the product: (first column) land surface models, (second column) reanalysis, and (third column) remote sensing derived products. Grey shading represents the uncertainty through the maximum and the minimum of the LF-data set. Units: mm/d.

throughout the year. However, in EQ and SAmz, both with small annual amplitude of radiation and abundant rainfall, the products show different shapes of the annual cycle and there is no clear relation between product category and shape. Here the representation of the annual cycles maintains a challenge.

3.2. Timing of Monthly Anomalies

A key application of ET products is the detection of hydrological variability, a more complex task than the simulation of the annual cycle. Here focus will be on the representation of ET monthly and seasonal anomalies and the associated uncertainties and relations to the drivers P and Rn.

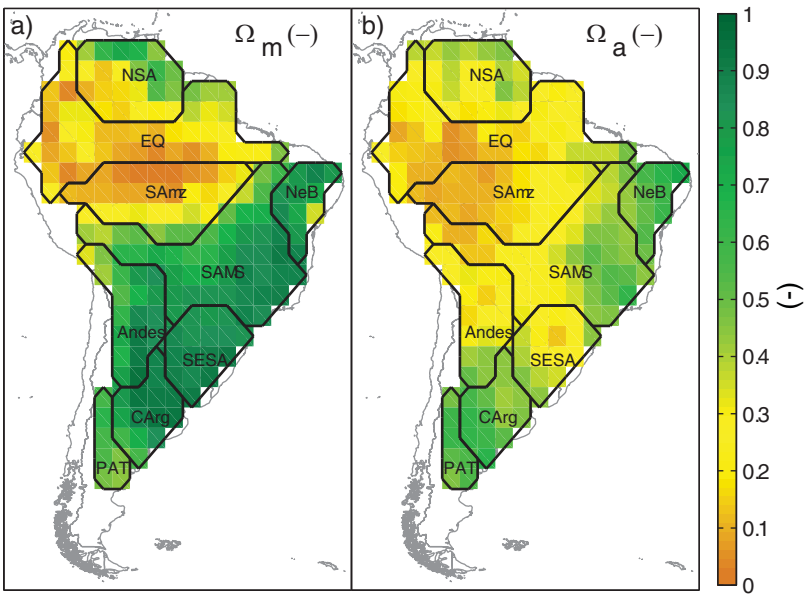

Figure 5. Maps of similarity index Ω, obtained from (a) monthly ET time series and (b) monthly anomaly ET time series. See section 2.4 for definition of Ω. Regions are drawn for a better interpretation of the results.

The monthly (or seasonal) anomalies are calculated subtracting the monthly mean of the period of study (1989–2005) from each monthly value. The relative monthly anomalies are then obtained by dividing the monthly anomaly with the monthly mean.

A synthesized picture of how well the ET products coincide on the representation of the temporal evolution of ET is defined by the similarity index Ω (section 2.4), displayed in Figure 5. The similarity of the time series of monthly means (Ωm, Figure 5a) shows a very clear general pattern with values above 0.7 to the southeast and low values to the northwest. Over parts of SAmz and EQ, the time series show no similarity at all and therefore, the choice of ET product for assessing any particular issue could be crucial for the outcome. For modeling studies over these regions that use ET as an input, it is essential to assess the sensitivity of the results to the ET product, and when evaluating a model that simulates ET, several ET products should be used. On the other hand, from NeB and southeastward until CArg, Ωm is as high as 0.7–0.9, indicating a low overall uncertainty and consequently the selection of a product for a particular study is less important. Patagonia also stands out with relatively low Ωm, probably due to the high uncertainty of the mean annual value of ET. As a complementary analysis, the Spearman correlations between each pair of products was calculated (not shown), but no clear relation between correlation and category of products was found. For example, while ERAI-L correlates well with ERAI, it also correlates well with LF-RS, but worse with the other three LSM products. The P-LSH RS product correlates better with LF-LSM, GLDAS2, and LF-REA than with LF-RS.

The similarity of the ET monthly anomalies (Ωa, Figure 5b) shows minimum the monsoon maximum; from the northern coasts of Brazil, westward over Amazonia and southeastward over the SESA region. It can be useful to look at Ωa before designing a study where the interannual variations of ET are particularly important for the outcome. For example, SESA stands out as a region with high Ωm but low Ωa. This means that the products agree well on the long term annual mean and on the amplitude and timing of the annual cycle, but not on monthly anomalies. In SESA the seasonal precipitation is dominated by internal variability and global climate models/reanalysis have poor skill in representing seasonal variability of precipitation (Nobre et al., 2006), consistent with low Ωa. On the contrary, some areas, like the eastern SAmz and southern CArg and PAT show higher Ωa than Ωm, meaning that the uncertainty of anomalies actually is lower than of the mean climate. The water-limited regions NeB, CArg, and PAT have the highest agreement in representing anomalies.

3.3. Can the ET Products Detect Droughts?

One of the most important applications of evapotranspiration monitoring is to estimate the severity of droughts (e.g., AghaKouchak et al., 2015; Crow et al., 2012). Here we will look at how the ET products

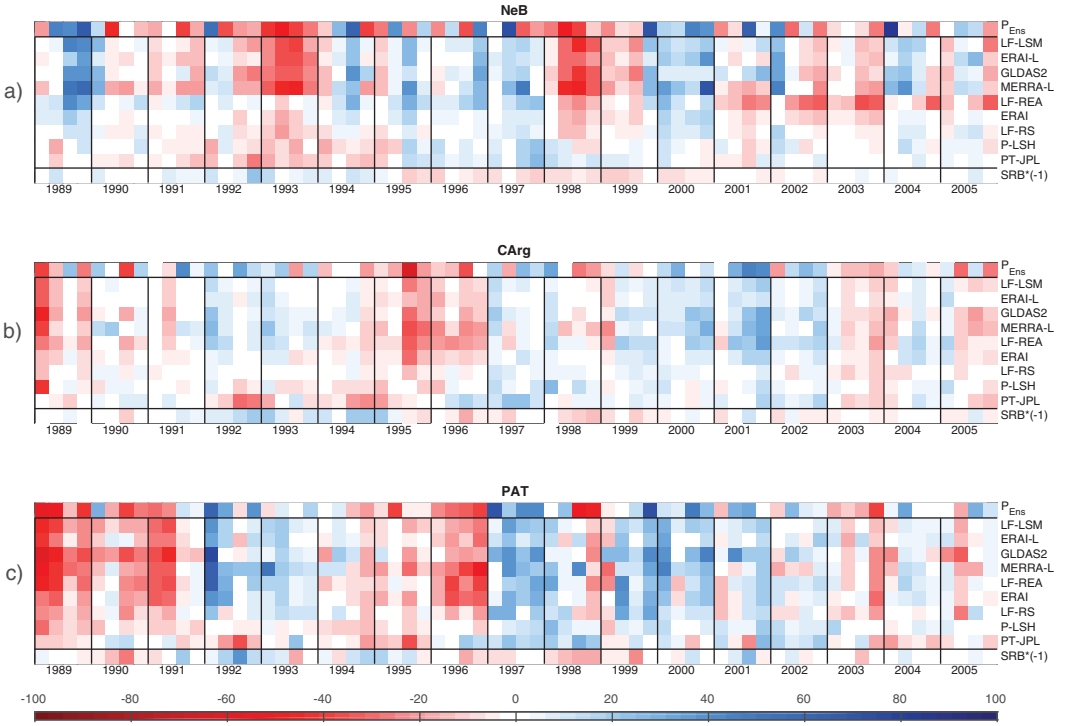

Figure 6. Time series of (top line) seasonal relative anomalies of P, (bottom line) all ET products and for SRB Rn for the supply-limited regions: (a) NeB, (b) CArg, and (c) PAT. (units: %). Positive (negative) P and ET anomalies are shown in blue (red) and positive (negative) Rn anomalies are shown in red (blue).

respond to meteorological drought (precipitation deficit) over three regions prone to suffer droughts that cause large socioeconomic damages: NeB, CArg, and PAT. We define meteorological drought by the seasonal anomaly of the mean time series of the four P products (see section 2.2). ET anomalies are actually more indicative of agricultural drought (negative anomalies of soil moisture, Van Loon 2015), which often is delayed with respect to meteorological drought (Van Loon, 2015; Van Loon & Van Lanen, 2012; Yang et al., 2014, 2017).While the P anomalies in Figure 6 only reveal meteorological and not agricultural drought, some severe agricultural droughts have been registered in literature and will be referred to in the following analysis. NeB (Figure 6a) suffered a precipitation deficit between 1990 and 1993 that lead to an agricultural drought in 1993 with mayor economic problems and human suffering (Rao et al., 1995) and the meteorological drought of 1997–1998 lead to an agricultural drought with 57% loss of the production (Marengo et al., 2017). The uncertainty of ET response is very large; the four LSM products respond strongly to both droughts with 20–50% of ET reduction while reanalysis and RS products respond with remarkably smaller reductions of 0–20%. Since no reference data set of "true" ET exists, we cannot say which product performs best, but for a product to be useful in a certain area, it should probably detect long and severe droughts reported in literature. Concerning the performance of LSMs, some recent studies have noticed that they overestimate the frequency or severity of drought events (De Kauwe et al., 2015; Tallaksen & Stahl, 2014; Ukkola et al., 2016). The reasons have to be examined for each individual LSM, but Ukkola et al. (2016) suggest two mechanisms that can cause this underestimation: (a) the soil hydrology (e.g., use of free drainage as lower soil moisture boundary condition, lack of groundwater and recharge zones) and (b) the representation of plant water stress (influence of vertical variations of soil moisture on plant uptake, failure to represent stress effects on both photosynthetic capacity and stomatal conductance). Reanalysis products use LSMs to calculate ET, so, given the same climatic situations it could be expected that they give similar response. However, here they show a weaker response, which could be a consequence of problems in the simulation of rainfall anomalies. In the case of LF-REA, the five last years of the series show a strong reduction in ET which is not evident in the GPCP precipitation or in the other ET products. It is out of the scope of this paper to analyze the causes, but it is an important example on how the use of only one ET product could give the erroneous result that this 5 year period was dryer than the droughts of 1993 and 1998. Weak

response of RS products to precipitation anomalies has also been found over Texas by Long et al. (2014) who used MODIS and AVHRR ET, both being Penman-Monteith approaches similar to the P-LSH product used here. Since these products rely heavily on vegetation features that do not respond immediately to increased water stress the response to soil moisture deficit can also be lagged (Rundquist & Harrington, 2000). In NeB, this effect can be seen in the P-LSH product for various strong dry/wet seasons, e.g., after the strong 1993 agricultural drought, P-LSH maintained a dry ET anomaly during the entire 1994 while LSMs immediately responded to increased precipitation in MAM 1994. In the case of the agricultural drought of 1998, the response of P-LSH is probably too weak and too delayed to be able to have generated the large losses of agricultural production reported in literature (Marengo et al., 2017). The PT-JPL product scales down the potential ET given by Priestly-Taylor equation to actual ET by using plant temperature and moisture constraint factors (Fisher et al., 2008). Since the PT-JPL product takes LST and total surface heat fluxes into account as net radiation, it could be expected that it would respond faster to meteorological drought than the P-LSH product. However, while the agricultural drought of 1993 is present in the PT-JPL product with a similar magnitude as LF-RS and P-LSH, the agricultural drought of 1998 is not detected at all. To understand if the failure to detect the agricultural drought of 1998 is due to the algorithm or to the forcing radiation, SRB seasonal anomalies are shown in the last line of Figure 6a (less Rn in blue and more Rn in red). It is clear that PT-JPL relies heavily on net radiation and that during 1997–1998 SRB registered a positive Rn anomaly which is the cause of the positive ET anomaly of the PT-JPL product. P-LSH also uses SRB as an input, but the algorithm relies more on NDVI than on Rn and it is therefore less evident to attribute the failure of P-LSH to represent the magnitude of the 1998 agricultural drought, but it could be a contributing cause.

CArg includes most of the areas exploited for agriculture and livestock in Argentina, a country whose economy relies heavily on grain exportation. Both flooding and droughts are recurrent and have devastating socioeconomic effects in the whole country. In 1995–1996, the worst drought since 1962 occurred (Llano & Penalba, 2011) which caused severe losses to agriculture and cattle during austral winter 1995 (Alessandro & Lichtenstein, 1996). In Figure 7b, the period SON 1994–SON 1996 is detected as anomalously dry by all the LSM and reanalysis products and also agrees on that the worst drought season occurred during austral winter 1995, coincident with the strongest precipitation anomaly. It should be noticed that the LSMs and reanalysis achieve this although they do not include processes potentially important for the variability of the surface climate of this region such as groundwater (Chen et al., 2010; Kuppel et al., 2015; Martinez et al., 2016) and vegetation dynamics (Müller et al., 2014). However, the analysis here is only qualitative and it is possible that these mechanisms are necessary for the products to represent the quantities of ET reduction correctly. For example, Chen et al. (2010) showed the importance of groundwater deficit for the severe drought in CArg of 2008–2009, a period which is not covered by our products. Their results indicate that the inclusion of groundwater in a LSM could be important since GLDAS, a LSM without groundwater, detects but underestimates the severity of the drought. To assess these issues there are urgent needs for both ground based measurements and model development. RS products show less coherence with the precipitation anomalies and with literature documenting the agricultural drought of 1995 (Alessandro & Lichtenstein, 1996; Llano & Penalba, 2011). In particular, after one and a half years of robust dry precipitation anomalies starting in SON 1994, in MAM 1996 all RS products cease to show dry anomalies. In the case of PT-JPL, this is related to the positive anomaly of SRB radiation (last line of Figure 6b). Only using RS products it would not be possible to distinguish 1995 as an extreme agricultural drought year. However, the agricultural drought of 2003, which was less severe than the one in 1995 but generated large losses in the agroindustry (Alessandro, 2008) is detected by all products, including RS products.

Droughts in PAT provoke losses of sheep which is the main livestock, fires, and eolic erosion. Agricultural droughts in PAT have not been reported in literature for the period of study, however it could be reasonable to assume soil moisture deficit after one or more years of precipitation deficit. The severest meteorological droughts during the analyzed period occurred in 1989–1991 and in 1996 and are detected with similar magnitudes by LSMs and Reanalysis (Figure 7c). LF-RS and P-LSH in general do detect these droughts (except for the zero response of P-LSH in 1996).The anomalies are weaker in RS products, which in itself does not mean erroneous, but the responses are similar to less extreme periods such as 1994–1995, not making it possible to distinguish between severe and weak droughts. PT-JPL show the lowest coherence with P anomalies, for example, 1990 and 1996, following long dry sequences have

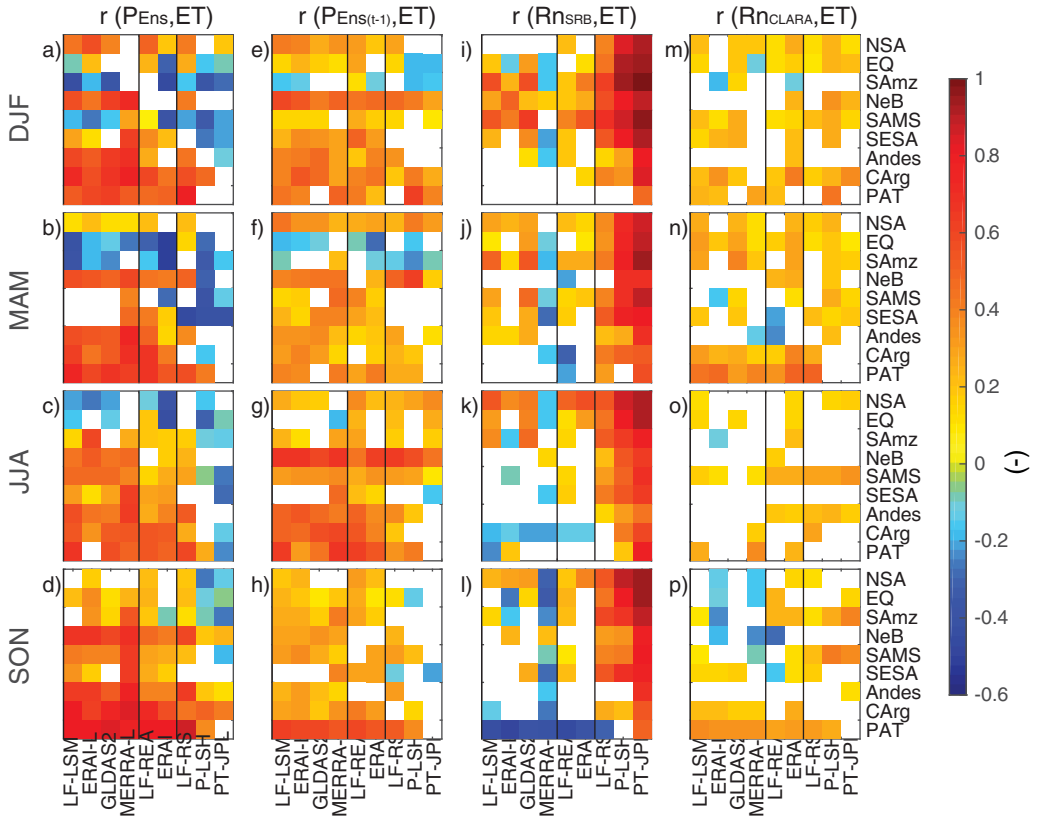

Figure 7. Correlations between seasonal anomalies of (first column, a–d) P_{Ens} and ET, (second column, e-h) P_{Ens} of the previous season, and (third column, i–l) ET and net surface radiation from SRB (Rn_{SRB}) and ET, and from (third column, m–p) CLARA (Rn_{CLARA}) and ET, for the four seasons (rows), are displayed in portrait diagrams of regions (rows in each portrait diagram) and ET data sets (columns in each portrait diagram). Vertical lines separate the categories of the products. White refers to nonsignificant correlation values at 95%.

weak wet anomalies which are coherent with SRB forcing radiation with positive anomalies. On the contrary 1992, which is a wet year in the P products is dry in PT-JPL due to negative SRB anomalies.

Some studies have reported a poor performance of the PM and PT algorithms in arid areas (Michel et al., 2016; Zhang et al., 2017). However here, at least in the case of PT-JPL, the SRB net radiation anomalies play an important role. In the next section the general relation between P, Rn, and ET anomalies are studied and a limited assessment of Rn uncertainty is realized.

3.4. ET Response to Precipitation and Radiation Anomalies

In section 3.3, we saw that LSM-based ET products respond stronger to precipitation anomalies than RS products in water-limited regions. Here we will look at the ET response to P and Rn seasonal anomalies for all regions, products and seasons. Since P-LSH and PT-JPL are forced with SRB, we also analyze an independent net radiation product, CLARA. Figure 7 displays portrait diagrams of the Spearman correlations (r) between seasonal anomalies of P_{Ens} and ET (a–d, first column) and between P_{Ens} of the preceding season and ET (e–h, second column), Rn of SRB (i–l, third column), and Rn of CLARA and ET (m–p, fourth column).

In the first column of Figure 7, we see that almost all products agree on the strong positive r(P_{Ens},ET) in the water-limited regions NeB, Andes, CArg, and PAT all year around and also for SAmz and SAMS during JJA (dry season) and SON (monsoon onset season). However, during seasons of abundant rainfall with related cloudiness, most products agree on a negative r(P_{Ens},ET), pointing out energy-limited regimes. This occurs in SAmz and SAMS (and to less extent in EQ) during the mature monsoon season DJF (Figure 7a), in EQ and SAmz during the declining monsoon season MAM (Figure 7b), for which rainfall still are abundant (see Figures 1b and 1c) as well as in NSA and EQ during JJA (Figure 7c), the rainy season in the northern part of the continent (Figure 1a). P-LSH and PT-JPL stands out by indicating a negative relation in most regions/

seasons, also for very dry cases such as NeB and CArg in MAM (P-LSH, Figure 7b) and CArg in JJA (PT-JPL, Figure 7c).

The lagged correlations r($P_{Ens(t-1)}$,ET) of the second column of Figure 7 are predominantly positive for all regions/seasons/products. In particular, the RS products show negative r($P_{Ens(t-1)}$,ET) only on few occasions in comparison to r(P_{Ens},ET). Comparing columns 1 and 2, it seems like the LSM-based products respond to P anomalies during the same season while RS products respond during the next season. ET anomalies can be lagged in comparison to P anomalies, as in the example of agricultural drought that lags meteorological drought (Van Loon, 2015). How long this lag is must differ from case to case, depending of land cover, temperature and strength of the anomaly. Without ground based evidence we cannot determine the correct response, except for in the cases of strong agricultural drought discussed in the previous section. With respect to the energy-limited regions with negative r(P_{Ens},ET), these mostly show positive lagged correlations, except for SAmz in DJF (Figure 7i) and EQ and SAmz in MAM (Figure 7j), which is partly due to positive autocorrelation of P_{Ens} (not shown).

Uncertainty of ET has multiple sources and one of them is the forcing Rn. Columns 3 and 4 of Figure 7 indicate that the representation of anomalies is very different between SRB and CLARA since they show different correlations with ET. P-LSH and PT-JPL correlate very well with SRB but not with CLARA, because the forcings of both products use SRB. Another outstanding difference is that SRB seems to correlate better with ET in energy-limited regions than in water-limited regions (which is what would be expected), while in CLARA we cannot make this generalization. An individual ET product with a distinctive behavior is MERRA-L with negative or nonsignificative r(Rn_{SRB},ET) for all regions except NeB which could be attributed to the different signs of the tendency of these time series.

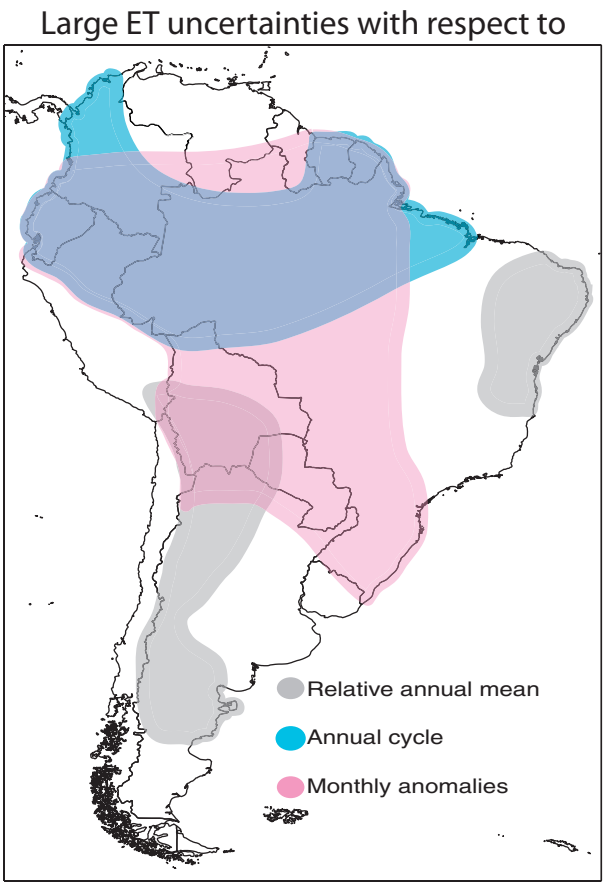

Figure 8. Schematic summary of the regions with largest uncertainty with respect to annual mean of ET (grey), annual cycle of ET (cyan), and representation of anomalies (pink).

4. Summary and Conclusions

The main objective of this paper was to give guidance to users of evapotranspiration (ET) products over South America by assessing their uncertainty and by highlighting strengths and weaknesses of some of the most common gridded products. To this end, an ensemble of nine products from land surface models (LSMs), reanalysis, and remote sensing data (RS) was analyzed with respect to their climatology, representation of anomalies and response to climatic forcing for the 1989–2005 reference period.

The spatial distribution of uncertainty depends on what metrics we are concerned with (Figure 8). The annual mean ET has a relative interproduct spread not smaller than 60% for any of the regions. This implies that studies that are concerned with annual mean ET, for example, climatological continental transport of moisture (such as van der Ent et al., 2010; Zemp et al., 2014) should run their models with different ET products to test the sensitivity to the input. Uncertainty of relative annual mean ET is even larger (close to 100%) in very dry, and which have large uncertainties in precipitation (Figure 8, grey color, regions NeB, PAT, and Andes). Uncertainties of the annual cycle are larger over energy-limited regions with an annual cycle of net surface radiation that is dominated by the precipitation annual cycle and not by the solar angle (Figure 8, cyan color, regions EQ and SAmz). Over these regions, in particular SAmz, the mechanisms that drive ET during the dry season are still poorly understood, and therefore it is not a surprise that products that rely on different theoretical considerations give different results. Finally, if our purpose is to represent strength and timing of monthly to seasonal hydrological anomalies, we should care about the largest uncertainty in the pink areas of Figure 8 (approximately regions EQ, SAmz, Andes, and SESA).

Table 2
Most Important Characteristics of Each ET Product

Product	Characteristics	
ERA-L GLDAS2	High-end estimation in water-limited regions.	Detect all droughts in dry regions. Overestimate drought magnitude?
MERRA-L	Avoid in NSA, EQ, Samz, and SAMS because of overestimation of ET during the wet season.	
LF-LSM	Low-end estimation in all regions, in particular in central Amazonia.	
ERAI LF-REA	High-end estimation in all regions.	
P-LSH	Low-end estimation in energy-limited regions. Avoid for studying droughts in water-limited regions because it does not distinguish between documented severe droughts and mild dry anomalies.	High-end estimation in NeB and Andes (water-limited regions with high radiation). Underestimate drought magnitude?
PT-JPL forced with SRB Rn	Avoid for studying droughts in water-limited regions because it does not distinguish between documented severe droughts and mild dry anomalies.	
LF-RS	Large spread in tropical regions. High-end estimation in arid regions.	

We also looked at the detection of droughts over three water-limited regions that are particularly affected on a socioeconomical level (NeB, CArg, and PAT). The LSM-based products, which are driven by observation-based corrected precipitation, detect all agricultural droughts reported in literature. However, although we cannot confirm this in our study, it is possible that the magnitude of ET reduction is overestimated (Ukkola et al., 2016). The possibility of overestimation of droughts by LSMs is quite a serious issue since ET is intrinsically related to surface temperature extremes through the coupling between latent and sensible heat fluxes. An underestimation of ET for periods of precipitation deficit would imply an overestimation of temperature which should be considered both in studies on heat extremes and in studies on climate change. This issue calls for efforts in comparing LSM results with observational in situ data over South America and to eventually use this information for development of model parameterizations.

When studying hydrological anomalies, not only the choice of individual ET product but also the category of product is crucial, since LSM-based products react immediately and strongly to precipitation anomalies, while the RS products used here show lagged responses with of less magnitude. While we suppose that agricultural drought lags meteorological drought in general, the real length of this lag is unknown and surely differ from case to case, making it impossible to generalize about if LSM-based or RS-based products perform better. The same is true regarding the magnitude of the anomalies. However, among four severe agricultural droughts reported in literature, the RS products only detect two. In the case of the PT-JPL product, we are confident that this is caused by the SRB forcing net radiation, which highlights the importance of uncertainties of radiation anomalies for the correct representation of ET anomalies.

The most important characteristics of the ET products are summarized in Table 2. Although the true ET is unknown hence making difficult the recommendation of individual products, clear outliers are marked. This is important knowledge when testing the sensitivity of a model to different products. In three cases, we feel confident in recommending not using a product, namely MERRA-L in the northern energy-limited regions and P-LSH and PT-JPL forced with SRB Rn in studies on agricultural droughts in the water-limited regions of South America.

References

Adler, R. F., Huffman, G. J., Chang, A., Ferraro, R., Xie, P., Janowiak, J., et al. (2003). The version 2 Global Precipitation Climatology Project (GPCP) monthly precipitation analysis (1979-present). *Journal of Hydrometeorology*, *4*, 1147–1167.

AghaKouchak, A., Farahmand, A., A., Melton, F. S., Teixeira, J., Anderson, M. C., Wardlow, B. D., et al. (2015). Remote sensing of drought: Progress, challenges and opportunities. *Reviews of Geophysics*, *53*, 452–480. https://doi.org/10.1002/2014RG000456

Acknowledgments
We acknowledge the projects LEFE/INSU AO2015–876370 (CNRS, France), Belmont Forum/ANR-15-JCL/-0002-01 "CLIMAX," PIP No 11220110100932 (CONICET, Argentina) and PICT 2014-0887 (ANPCyT, Argentina). We thank Jerónimo Escribano for discussions about clustering techniques and Pablo Zaninelli for comments on the manuscript. GPCP is publicly available from NOAA: https://www.esrl.noaa.gov/psd/data/gridded/data.gpcp.html; UDEL from NOAA: https://www.esrl.noaa.gov/psd/data/gridded/data.Udel_AirT_Precip.html; CPC-UNI from NOAA: https://www.esrl.noaa.gov/psd/data/gridded/data.cpc.globalprecip.html;CRU; from British Atmospheric Data Centre RAL: http://badc.nerc.ac.uk/data/cru/; SRBfrom NASA LaRC/GEWEX SRB: https://eosweb.larc.nasa.gov/project/srb/srb_table; CLARA from EUMETSAT through NCAR/UCAR: https://climatedataguide.ucar.edu/climate-data/clara-a1-cloud-properties-surface-albedo-and-surface-radiation-products-based-avhrr; LandFlux-EVAL from ETHzürich: http://www.iac.ethz.ch/group/land-climate-dynamics/research/landflux-eval.html; ERA Interim/Land from ECMWF: http://apps.ecmwf.int/datasets/data/interim-land/type=fc/; ERA Interim from ECMWF: http://apps.ecmwf.int/datasets/data/interim-mdfa/levtype=sfc/; GLDAS2 from NASA: https://hydro1.gesdisc.eosdis.nasa.gov/data/GLDAS/GLDAS_NOAH025_M.2.0/; MERRA-L from NASA: https://gmao.gsfc.nasa.gov/reanalysis/MERRA/merra-land.php; P-LSH from NASA: https://webmap.ornl.gov/ogc/dataset.jsp?ds_id=10020; PT-JPL from LandFlux.org: http://landflux.org/Data.php.

Alessandro, A. P. (2008). Anomalías de circulación atmosférica en 500 y 1000 hPa asociada a la sequía producida en la Argentina durante enero de 2003 a marzo de 2004. *Revista Brasileira de Meteorologia*, *23*(1), 12–29.
Alessandro, P., & Lichtenstein, E. (1996). Situación sinóptica asociada a la sequía del invierno de 1995. *Revista Geofísica*, *45*, 125–1443.
Baldocchi, D., Falge, E., Gu, L., Olson, R., Hollinger, D., Running, S., et al. (2001). FLUXNET: A new tool to study the temporal and spatial variability of ecosystem-scale carbon dioxide, water vapor, and energy flux densities. *Bulletin of the American Meteorological Society*, *82*, 2415–2434.
Balsamo, G., Albergel, C., Beljaars, A., Boussetta, S., Brun, E., Cloke, H., et al. (2015). ERA-Interim/Land: A global land surface reanalysis data set. *Hydrology and Earth System Sciences*, *19*, 389–407. https://doi.org/10.5194/hess-19-389-2015
Balsamo, G., Viterbo, P., Beljaars, A., van den Hurk, B., Hirschi, M., Betts, A. K., et al. (2009). A revised hydrology for the ECMWF model: Verification from field site to terrestrial water storage and impact in the Integrated Forecast System. *Journal of Hydrometeorology*, *10*, 623–643.
Barros V., Clarke, R., Silva Dias, P. (Eds.) (2003). Climate change in the la Plata Basin. In *SGP II 057: Trends in the hydrological cycle of the Plata basin: Raising awareness and new tools for water management*. Inter American Institute on Global Change (IAI).
Boé, J., & Terray, L. (2008). Uncertainties in summer evapotranspiration changes over Europe and implications for regional climate change. *Geophysical Research Letters*, *35*, L05702. https://doi.org/10.1029/2007GL032417
Budyko, M. I. (1982). *1982: The Earth's climate: Past and future* (307 pp.). New York, NY: Academic.
Chen, J. L., Wilson, C. R., Tapley, B. D., Longuevergne, L., Yang, Z. L., & Scanlon, B. R. (2010). Recent La Plata basin drought conditions observed by satellite gravimetry. *Journal of Geophysical Research*, *115*, D22108. https://doi.org/10.1029/2010JD014689
Chen, M., Xie, P., & CPC Precipitation Working Group. (2008). *CPC unified gauge-based analysis of global daily precipitation*. Paper presented at the Western Pacific Geophysics Meeting, Cairns, Australia, 29 July to 1 August 2008.
Christoffersen, B. O., Restrepo-Coupe, N., Altaf Arain, M., Baker, I. T., Cestaro, B. P., Ciais, P., et al. (2014). Mechanisms of water supply and vegetation demand govern the seasonality and magnitude of evapotranspiration in Amazonia and Cerrado. *Agricultural and Forest Meteorology*, *191*(15), 33–50.
Costa, M. H., Biajoli, M. C., Sanches, L., Malhado, A. C. M., Hutyra, L. R., da Rocha, H. R., et al. (2010). Atmospheric versus vegetation controls of Amazonian tropical rain forest evapotranspiration: Are the wet and seasonally dry rain forests any different? *Journal of Geophysical Research*, *115*, G04021. https://doi.org/10.1029/2009JG001179
Crow, W. T., Kumar, S. V., & Bolten, J. D. (2012). On the utility of land surface models for agricultural drought monitoring. *Hydrology and Earth System Sciences*, *16*, 3451–3460.
Dee, D. P., Uppala, S. M., Simmons, A. J., Berrisford, P., Poli, P., Kobayashi, S., et al. (2011). The ERA-Interim reanalysis: Configuration and performance of the data assimilation system. *Quarterly Journal of the Royal Meteorological Society*, *137*, 553–597. https://doi.org/10.1002/qj.828
De Kauwe, M. G., Zhou, S.-X., Medlyn, B. E., Pitman, A. J., Wang, Y. P., Duursma, R. A., et al. (2015). Do land surface models need to include differential plant species responses to drought? Examining model predictions across a latitudinal gradient in Europe. *Biogeosciences*, *12*, 12349–12393.
Dirmeyer, P. A., Brubaker, K. L., & DelSole, T. (2009). Import and export of atmospheric water vapor between nations. *Journal of Hydrology*, *365*, 11–22.
Ek, M. B., Mitchell, K. E., Lin, Y., Rogers, E., Grunmann, P., Koren, V., et al. (2003). Implementation of Noah land surface model advances in the National Centers for Environmental Prediction operational mesoscale Eta Model. *Journal of Geophysical Research*, *108*(D22), 8851. https://doi.org/10.1029/2002JD003296
Fisher, J. B., Malhi, Y., Bonal, D., da Rocha, H. R., de Araújo, A. C., Gamo, M., et al. (2009). The land-atmosphere water flux in the tropics. *Global Change Biology*, *15*, 2694–2714.
Fisher, J. B., Tu, K. P., & Baldocchi, D. D. (2008). Global estimates of the land-atmosphere water flux based on monthly AVHRR and ISLSCP-II data, validated at 16 FLUXNET sites. *Remote Sensing of Environment*, *112*(3), 909–919.
Germer, S., Neill, C., Vetter, T., Chaves, J., Krusche, A. V., & Elsenbeer, H. (2009). Implications of longterm land use change for the hydrology and solute budgets of small catchments in Amazonia. *Journal of Hydrology*, *364*, 349–363.
Getirana, A. C. V., Dutra, E., Guimberteau, M., Kam, J., Li, H.-Y., Decharme, B., et al. (2014). Water balance in the Amazon basin from a land surface model ensemble. *Journal of Hydrometeorology*, *15*, 2586–2614.
Glenn, E., Nagler, P., & Huete, A. (2010). Vegetation index methods for estimating evapotranspiration by remote sensing. *Surveys in Geophysics*, *31*(6), 531–555.
Hamilton, S. (2002). *Hydrological controls of ecological structure and function in the Pantanal Wetland (Brazil). The ecohydrology of South American Rivers and Wetlands* (IAHS Spec. Publ. 6).
Harris, I. C., & Jones, P. D. (2015). *CRU TS3.23: Climatic Research Unit (CRU) time-series (TS) version 3.23 of high resolution gridded data of month-by-month variation in climate (Jan. 1901–Dec. 2014)*. Centre for Environmental Data Analysis. Retrieved from https://doi.org/10.5285/4c7fdfa6-f176-4c58-acee-683d5e9d2ed5
Hirschi, M., Seneviratne, S. I., Alexandrov, V., Boberg, F., Boroneant, C., Christensen, O. B., et al. (2011). Observational evidence for soil-moisture impact on hot extremes in southeastern Europe. *Nature Geoscience*, *4*(1), 17–21.
Jiménez, C., Prigent, C., Mueller, B., Seneviratne, S., McCabe, M., Wood, E., et al. (2011). Global intercomparison of 12 land surface heat flux estimates. *Journal of Geophysical Research*, *116*, D02102. https://doi.org/10.1029/2010JD014545
Jung, M., Reichstein, M., & Bondeau, A. (2009). Towards global empirical upscaling of FLUXNET eddy covariance observations: Validation of a model tree ensemble approach using a biosphere model. *Biogeosciences*, *6*, 2001–2013.
Jung, M., Reichstein, M., Ciais, P., Seneviratne, S. I., Sheffield, J., Goulden, M. L., et al. (2010). Recent decline in the global land evapotranspiration trend due to limited moisture supply. *Nature*, *467*, 951–954.
Kalma, J. D., McVicar, T. R., & McCabe, M. F. (2008). Estimating land surface evaporation: A review of methods using remotely sensed surface temperature data. *Surveys in Geophysics*, *29*, 421–469.
Kalnay, E., Kanamitsu, M., Kistler, R., Collins, W., Deaven, D., Gandin, L., et al. (1996). The NCEP/NCAR 40-year reanalysis project. *Bulletin of the American Meteorological Society*, *77*, 437–471.
Karlsson, K.-G., Riihelä, A., Müller, R., Meirink, J. F., Sedlar, J., Stengel, M., et al. (2013). CLARA-A1: A cloud, albedo, and radiation dataset from 28 yr of global AVHRR data. *Atmospheric Chemistry and Physics*, *13*, 5351–5367.
Koster, R. D., Suarez, M. J., Ducharne, A., Stieglitz, M., & Kumar, P. (2000). A catchment-based approach to modeling land surface processes in a general circulation model 1. Model structure. *Journal of Geophysical Research*, *105*(D20), 24809–24822.
Kuppel, S., Houspanossian, J., Nosetto, M. D., & Jobbágy, E. G. (2015). What does it take to flood the Pampas?: Lessons from a decade of strong hydrological fluctuations. *Water Resources Research*, *51*, 2937–2950. https://doi.org/10.1002/2015WR016966

Li, W., & Fu, R. (2004). Transition of the large-scale atmospheric and land surface conditions from the dry to the wet season over Amazonia as diagnosed by the ECMWF Re-Analysis. *Journal of Climate*, *17*, 2637–2651.
Lima, L. S., Coe, M. T., Soares Filho, B. S., Cuadra, S. V., Dias, L. C., Costa, M. H., et al. (2014). Feedbacks between deforestation, climate, and hydrology in the Southwestern Amazon: Implications for the provision of ecosystem services. *Landscape Ecology*, *29*, 261–274.
Llano, M. P., & Penalba, O. C. (2011). A climatic analysis of dry sequences in Argentina. *International Journal of Climatology*, *31*, 504–513.
Loew, A., Andersson, A., Trentmann, J., & Schröder, M. (2016). Assessing surface solar radiation fluxes in the CMIP ensembles. *Journal of Climate*, *29*(20), 7231–7246.
Long, D., Longuevergne, L., & Scanlon, B. R. (2014). Uncertainty in evapotranspiration from land surface modeling, remote sensing, and GRACE satellites. *Water Resources Research*, *50*, 1131–1151. https://doi.org/10.1002/2013WR014581
Los, S. O., Collatz, G. J., Malmstrom, C. M., Pollack, N. H., DeFries, R. S., Bounoua, L., et al. (2000). A global 9-year biophysical land surface dataset from NOAA AVHRR data. *Journal of Hydrometeorology*, *1*, 183–−199.
Loveland, T. R., Reed, B. C., Brown, J. F., Ohlen, D. O., Zhu, Z., Youing, L., et al. (2000). Development of a global land cover characteristics database and IGB6 DISCover from the 1 km AVHRR data. *International Journal of Remote Sensing*, *21*, 1303–1330.
Marengo, J. A., & Bernasconi, M. (2015). Regional differences in aridity/drought conditions over Northeast Brazil: Present state and future projections. *Climatic Change*, *129*, 103.
Marengo, J. A., Torres, R. R., & Alves, L. M. (2017). Drought in Northeast Brazil—Past, present, and future. *Theoretical and Applied Climatology*, *129*, 1189–1200. https://doi.org/10.1007/s00704-016-1840-8
Martinez, J. A., & Dominguez, F. (2014). Sources of atmospheric moisture for the La Plata River Basin. *Journal of Climate*, *27*, 6737–6753.
Martinez, J. A., Dominguez, F., & Miguez-Macho, G. (2016). Effects of a groundwater scheme on the simulation of soil moisture and evapotranspiration over southern South America. *Journal of Hydrometeorology*, *17*, 2941–2957. https://doi.org/10.1175/JHM-D-16-0051.1
Masiokas, M., Villalba, R., & Luckman, B. (2006). Snowpack variations in the central Andes of Argentina and Chile, 1951–2005: Large-scale atmospheric influences and implications for water resources. *Journal of Climate*, *19*, 6334–6352.
Masiokas, M. H., Rivera, A., Espizua, L. E., Villalba, R., Delgado, S., & Aravena, J. C. (2009). Glacier fluctuations in extratropical South America during the past 1000 years. *Palaeogeography, Palaeoclimatology, Palaeoecology*, *281*, 242–268.
Masson, V., Champeaux, J.-L., Chauvin, F., Meriguet, C., & Lacaze, R. (2003). A global database of land surface parameters at 1-km resolution in meteorological and climate models. *Journal of Climate*, *16*, 1261–1282.
Mecikalski, J. R., Diak, G. R., Anderson, M. C., & Norman, J. M. (1999). Estimating fluxes on continental scales using remotely sensed data in an atmospheric–land exchange model. *Journal of Applied Meteorology*, *38*, 1352–1369.
Michel, D., Jiménez, C., Miralles, D. G., Jung, M., Hirschi, M., Ershadi, A., et al. (2016). The WACMOS-ET project—Part 1: Tower-scale evaluation of four remote-sensing-based evapotranspiration algorithms. *Hydrology and Earth System Sciences*, *20*(2), 803–822. https://doi.org/10.5194/hess-20-803-2016
Miguez-Macho, G., & Fan, Y. (2012). The role of groundwater in the Amazon water cycle: 2. Influence on seasonal soil moisture and evapotranspiration. *Journal of Geophysical Research*, *117*, D15114. https://doi.org/10.1029/2012JD017540
Miralles, D. G., Jiménez, C., Jung, M., Michel, D., Ershadi, A., McCabe, M. F., et al. (2016). The WACMOS-ET project—Part 2: Evaluation of global terrestrial evaporation data sets. *Hydrology and Earth System Sciences*, *20*, 823–842.
Mueller, B., Hirschi, M., Jiménez, C., Ciais, P., Dirmeyer, P. A., Dolman, A. J., et al. (2013). Benchmark products for land evapotranspiration: LandFlux-EVAL multi-data set synthesis. *Hydrology and Earth System Sciences*, *17*, 3707–3720.
Mueller, B., Hirschi, M., & Seneviratne, S. I. (2011). New diagnostic estimates of variations in terrestrial water storage based on ERA-Interim data. *Hydrological Processes*, *25*, 996–1008.
Mueller, B., & Seneviratne, S. I. (2012). Hot days induced by precipitation deficits at the global scale. *Proceedings of the National Academy of Sciences of the United States of America*, *109*(31), 12398–12403.
Müller, O., Berbery, E. H., Alcaraz-Segura, D., & Ek, M. B. (2014). Regional model simulations of the 2008 drought in South America using a consistent set of land surface properties. *Journal of Climate*, *27*, 6754–6778.
Nobre, P., Marengo, J. A., Cavalcanti, I. F. A., Obregon, G., Barros, V., Camilloni, I., et al. (2006). Seasonal-to-decadal predictability and prediction of South American climate. *Journal of Climate*, *19*(23), 5988–6004.
Nosetto, M. D., Paez, R. A., Ballesteros, S. I., & Jobbágy, E. G. (2015). Higher water-table levels and flooding risk under grain vs. livestock production systems in the subhumid plains of the Pampas. *Agriculture, Ecosystems and Environment*, *206*, 60–70.
Pinzon, J., Brown, M. E., & Tucker, C. J. (2005). Satellite time series correction of orbital drift artifacts using empirical model decomposition. In N. E. Huang & S. S. P. Shen (Eds.), *Hilbert-Huang transform: Introduction and applications* (pp.167–186). Singapore: World Scientific.
Pitman, A. J. (2003). The evolution of, and revolution in, land surface schemes designed for climate models. *International Journal of Climatology*, *23*, 479–510.
Rao, V. B., Hada, K., & Herdies, D. (1995). On the severe drought of 1993 in north-east Brazil. *International Journal of Climatology*, *15*(6), 697–704.
Reichle, R. H., Koster, R. D., De Lannoy, G. J. M., Forman, B. A., Liu, Q., Mahanama, S. P. P., et al. (2011). Assessment and enhancement of MERRA land surface hydrology estimates. *Journal of Climate*, *24*, 6322–6338.
Rienecker, M. M., Suarez, M. J., Gelaro, R., Todling, R., Bacmeister, J., Liu, E., et al. (2011). MERRA: NASA's Modern-Era Retrospective Analysis for Research and Applications. *Journal of Climate*, *24*, 3624–3648.
Rivera, J. A., Penalba, O., & Bettolli, M. (2013). Inter-annual and inter-decadal variability of dry days in Argentina. *International Journal of Climatology*, *33*, 834–842.
Rodell, M., Houser, P., Jambor, U., Gottschalck, J., Mitchell, K., Meng, C., et al. (2004). The Global Land Data Assimilation System. *Bulletin of the American Meteorological Society*, *85*, 381–394.
Rundquist, B. C., & Harrington, J. A., Jr., (2000). The effects of climatic factors on vegetation dynamics of tallgrass and shortgrass cover. *GeoCarto International*, *15*, 31–36.
Ruscica, R. C., Menéndez, C. G., & Sörensson, A. A. (2016). Land surface–atmosphere interaction in future South American climate using a multi-model ensemble. *Atmospheric Science Letters*, *17*, 141–147.
Ruscica, R. C., Sörensson, A. A., & Menéndez, C. G. (2015). Pathways between soil moisture and precipitation in southeastern South America. *Atmospheric Science Letters*, *16*(3), 267–272.
Seneviratne, S. I., Corti, T., Davin, E. L., Jaeger, E. B., Hirschi, M., Lehner, I., et al. (2010). Investigating soil moisture-climate interactions in a changing climate: A review. *Earth-Science Reviews*, *99*(3–4), 125–161.
Seneviratne, S. I., Luethi, D., Litschi, M., & Schär, C. (2006). Land-atmosphere coupling and climate change in Europe. *Nature*, *443*, 205–209.
Sheffield, J., Goteti, G., & Wood, E. F. (2006). Development of a 50-year high resolution global dataset of meteorological forcings for land surface modeling. *Journal of Climate*, *19*, 3088–3111. https://doi.org/10.1175/JCLI3790.1

Silveira, L., & Alonso, J. (2009). Runoff modifications due to the conversion of natural grasslands to forests in a large basin in Uruguay. *Hydrological Processes*, *23*, 320–329.
Stackhouse, P. W., Gupta, S. K., Hall, F. G., Collatz, G. J., Meeson, B. W., Los, S. O., et al. (2013). *ISLSCP II Surface Radiation Budget (SRB) Radiation Data*. Oak Ridge, TN: ORNL DAAC. https://doi.org/10.3334/ORNLDAAC/1201
Stackhouse, P. W., Gupta, S. K., Cox, S. J., Zhang, T., Mikovitz, J. C., & Hinkelman, L. M. (2011). 24.5-year data set released. *GEWEX News*, 21(1), 10–12.
Tallaksen, L. M., & Stahl, K. (2014). Spatial and temporal patterns of large-scale droughts in Europe: Model dispersion and performance. *Geophysical Research Letters*, *41*, 429–434. https://doi.org/10.1002/2013GL058573
Teuling, A. J., Van Loon, A. F., Seneviratne, S. I., Lehner, I., Aubinet, M., Heinesch, B., et al. (2013). Evapotranspiration amplifies European summer drought. *Geophysical Research Letters*, *40*, 2071–2075. https://doi.org/10.1002/grl.50495
Ukkola, A. M., Pitman, A. J., Decker, M., De Kauwe, M. G., Abramowitz, G., Kala, J., et al. (2016). Modelling evapotranspiration during precipitation deficits: Identifying critical processes in a land surface model. *Hydrology and Earth System Sciences*, *20*, 2403–2419.
van der Ent, R. J., Savenije, H. H. G., Schaefli, B., & Steele-Dunne, S. C. (2010). Origin and fate of atmospheric moisture over continents. *Water Resources Research*, *46*, W09525. https://doi.org/10.1029/2010WR009127
Van Loon, F., & Van Lanen, H. A. J. (2012). A process-based typology of hydrological drought. *Hydrology and Earth System Sciences*, *16*, 1915–1946. https://doi.org/10.5194/hess-16-1915-2012
Van Loon, A. F. (2015). Hydrological drought explained. *WIREs Water*, *2*, 359–392. https://doi.org/10.1002/wat2.1085
Vinukollu, R. K., Meynadier, R., Sheffield, J., & Wood, E. F. (2011). Multi-model, multi-sensor estimates of global evapotranspiration: Climatology, uncertainties and trends. *Hydrological Processes*, *25*, 3993–4010.
Viterbo, P., & Beljaars, A. C. M. (1995). *An improved land surface parametrization scheme in the ECMWF model and its validation* (Tech. Rep. 75). Reading, UK: ECMWF.
Wang, K., & Dickinson, R. E. (2012). A review of global terrestrial evapotranspiration: Observation, modeling, climatology, and climatic variability. *Reviews of Geophysics*, *50*, RG2005. https://doi.org/10.1029/2011RG000373
Willmott, C. J., & Matsuura, K. (2001). *Terrestrial air temperature and precipitation: Monthly and annual time series (1950–1999)*. Retrieved from http://climate.geog.udel.edu/~climate/html_pages/README.ghcn_ts2.html
Wu, J., Albert, L. P., Lopes, A. P., Restrepo-Coupe, N., Hayek, M., Wiedemann, K. T., et al. (2016). Leaf development and demography explain photosynthetic seasonality in Amazon evergreen forests. *Science*, *351*, 972–976.
Yamada, T. J., Koster, R. D., Kanae, S., & Oki, T. (2007). Estimation of predictability with a newly derived index to quantify similarity among ensemble members. *Monthly Weather Review*, *135*, 2674–2687.
Yang, Y., Donohue, R. J., & McVicar, T. R. (2016). Global estimation of effective plant rooting depth: Implications for hydrological modeling. *Water Resources Research*, *52*, 8260–8276. https://doi.org/10.1002/2016WR019392
Yang, Y., Long, D., Guan, H., Liang, W., Simmons, C., & Batelaan, O. (2015). Comparison of three dual-source remote sensing evapotranspiration models during the MUSOEXE-12 campaign: Revisit of model physics. *Water Resources Research*, *51*, 3145–3165. http://dx.doi.org/10.1002/2014WR015619
Yang, Y., Long, D., Guan, H., Scanlon, B. R., Simmons, C. T., Jiang, L., et al. (2014). GRACE satellite observed hydrological controls on interannual and seasonal variability in surface greenness over mainland Australia. *Journal of Geophysical Research: Biogeosciences*, *119*, 2245–2260. https://doi.org/10.1002/2014JG002670
Yang, Y., McVicar, T. R., Donohue, R. J., Zhang, Y., Roderick, M. L., Chiew, F. H. S., et al. (2017). Lags in hydrologic recovery following an extreme drought: Assessing the roles of climate and catchment characteristics. *Water Resources Research*, *53*, 4821–4837. https://doi.org/10.1002/2017WR020683
Yin, D., Roderick, M. L., Leech, G., Sun, F., & Huang, Y. (2014). The contribution of reduction in evaporative cooling to higher surface air temperatures during drought. *Geophysical Research Letters*, *41*, 7891–7897. https://doi.org/10.1002/2014GL062039
Zemp, D. C., Schleussner, C.-F., Barbosa, H. M. J., van der Ent, R. J., Donges, J. F., Heinke, J., et al. (2014). On the importance of cascading moisture recycling in South America. *Atmospheric Chemistry and Physics*, *14*, 13337–13359.
Zhang, K., Kimball, J. S., Nemani, R. R., & Running, S. W. (2010). A continuous satellite-derived global record of land surface evapotranspiration from 1983 to 2006. *Water Resources Research*, *46*, W09522. https://doi.org/10.1029/2009WR008800
Zhang, K., Ma, J., Zhu, G., Ma, T., Han, T., & Feng, L. L. (2017). Parameter sensitivity analysis and optimization for a satellite-based evapotranspiration model across multiple sites using Moderate Resolution Imaging Spectroradiometer and flux data. *Journal of Geophysical Research: Atmospheres*, *122*, 230–245. https://doi.org/10.1002/2016JD025768
Zhang, T., Stackhouse, P. W., Gupta, S. K., Cox, S. J., Colleen Mikovitz, J., & Hinkelman, L. M. (2013). The validation of the GEWEX SRB surface shortwave flux data products using BSRN measurements: A systematic quality control, production and application approach. *Journal of Quantitative Spectroscopy & Radiative Transfer*, *122*, 127–140.